Available online at www.sciencedirect.com

ScienceDirect

journal homepage: www.elsevier.com/locate/he

Modelling hydrogen production by the rich combustion of heavy fuel oil

J. Gómez [a], J.P. Mmbaga [c], R.E. Hayes [c,**], M. Toledo [b,*], F. Gracia [a]

[a] Department of Chemical Engineering and Biotechnology, Facultad de Ciencias Físicas y Matemáticas, Universidad de Chile, Beauchef 850, Santiago, Chile

[b] Department of Mechanical Engineering, Universidad Técnica Federico Santa María, Av. España 1680, Valparaíso, Chile

[c] Department of Chemical and Materials Engineering, University of Alberta, Edmonton, Alberta, Canada

ARTICLE INFO

Article history:
Received 21 July 2016
Accepted 16 August 2016
Available online 2 September 2016

Keywords:
Filtration combustion
Partial oxidation reforming
Heterogeneous modelling
Decalin
Heavy fuel oil
Syngas

ABSTRACT

This paper reports on a modelling study of the rich combustion of heavy fuel oil in a reactor packed with an inert porous medium. Decalin is used as a model compound to represent the heavy fuel oil. A computational model is developed for the reactor, based on a two space dimensional transient heterogeneous description, and a kinetic global model for partial oxidation reforming of decalin is proposed. Also, equilibrium calculations were performed for the experimental conditions of the study. The experimental and simulation results show that heavy fuel oil is a potential fuel to produce hydrogen. It is concluded that notable characteristics of the process can be observed by simulation: the presence of an axial maximum in the production of H_2, and positive effects of the equivalence ratio and filtration velocity increase and heat losses reduction on the fuel conversion to H_2.

© 2016 Hydrogen Energy Publications LLC. Published by Elsevier Ltd. All rights reserved.

Introduction

Synthesis gas, also known as syngas, is a mixture of hydrogen and carbon monoxide that is extensively used as a chemical feedstock, as well as being an important source of hydrogen. It can also be used for enrichment of traditional combustors, or as a way to produce a high quality fuel from a feed of low energy content or from carbon neutral sources (e.g. biodiesel, vegetable oil, and waste oil). Syngas can also be used to generate electricity by direct combustion, for the operation of high-temperature fuel cells (MCFC and SOFC), or in the production of value added chemicals (e.g. methanol, higher alcohols, detergents and ammonia) [1,2]. Syngas can be produced from various hydrocarbon sources, including natural gas, liquefied petroleum gas (LPG), fuel liquids, coal and biomass. The partial oxidation of liquid fuels is a promising method for hydrocarbon production, and its use in reactors containing an inert porous medium (IPM) has garnered considerable interest over the last 20 years. The use of an IPM for homogeneous gas phase reactions is known as filtrational gas combustion. During this process, the combustion reaction occurring in the porous medium can be described by one of the following steady-state regimes, which in turn depend on the propagation velocity of the thermal wave. The *low-velocity regime* (LVR) has flame propagation velocities of the order of 10^{-4} m/s, whilst the *high-velocity regime* (HVR) has a wave velocity of approximately 10 m/s. In the *sound velocity regime*

* *Corresponding author.*
** *Corresponding author.* Fax: +1 780 4922881.
E-mail addresses: bob.hayes@ualberta.ca (R.E. Hayes), mario.toledo@usm.cl (M. Toledo).
http://dx.doi.org/10.1016/j.ijhydene.2016.08.111
0360-3199/© 2016 Hydrogen Energy Publications LLC. Published by Elsevier Ltd. All rights reserved.

(SVR) the wave velocity is approximately 100 m/s. As the wave velocity increases, we encounter the low-velocity detonation (LVD) at 800–1500 m/s followed by the normal detonation with losses region (ND) at 1500–2000 m/s [3].

The inert porous medium in the reactor usually consists of pellets of varying geometries that are randomly packed. Heat transfer effects are especially important in the bed, and occur by conduction and radiation between the particle surfaces, and by convection between the solid and gas [4,5]. The reactions and heat transfer mechanisms control the temperature, which may differ significantly from the adiabatic value. The reactors can be operated in either the stationary or transient mode. Steady state operation is widely practised in radiant burners and surface combustor-heaters, where the combustion zone is stabilized within the finite element of the porous matrix. Transient operation involves a travelling wave representing a zone of transient combustion freely propagating in either the upstream or downstream direction within the porous medium [5].

Dixon et al. [6] studied the conversion of liquid heptane to syngas in a packed bed reactor containing alumina pellets. The heptane feed was vaporized with air. The experimental and numerical investigations focused on the effects of the equivalence ratio (φ) and the inlet velocity on the outlet composition. The equivalence ratio is defined as the ratio of the stoichiometric air flow rate and the actual air flow. With constant input velocity, the hydrogen production increased with an increase of equivalence ratio, and hydrogen conversion efficiency reached its maximum value when φ was approximately equal to 3.0. Tests at a constant equivalence ratio of 2.5 showed that the conversion efficiency increased with the inlet velocity, and at the highest velocity tested of 80 cm/s, the experimental values exceeded 80%. Similar trends were observed for carbon monoxide conversion and energy efficiencies, with maximum values that exceeded 90 and 80% respectively. Overall, the results indicated that favourable conditions for fuel reforming are with φ of 2.5–3.5, and showed that the inlet velocity has a significant effect on the performance. There was a substantial gain in efficiency with the increase in the inlet velocity, which was attributed to the increase in the temperature of the reactor.

The works of Pedersen-Mjaanes et al. [7] and Pastore and Mastorakos [8] on super-adiabatic combustion of liquids (methanol, octane and n-heptane, among others) in a two-layer porous burner with steady rich stabilized flames demonstrated the capacity to produce syngas rich in hydrogen. In particular, Pastore and Mastorakos [9] investigated the rich combustion of n-heptane, diesel oil, kerosene and rapeseed-oil methyl ester (RME) biodiesel, for the purpose of producing syngas for fuel cells applications, or for the enrichment of traditional combustion chambers. The rich flames were stabilized in a combustor of inert porous media with two-layers and were examined over a range of equivalence ratios and porous materials. The n-heptane was successfully reformed until a value of φ equal to 3.0, reaching a conversion efficiency (based on the lower heating value of H_2 and CO over the fuel input) up to 75% for a packed bed of alumina beads. Similarly, diesel, kerosene and biodiesel were reformed to syngas in a zirconia foam burner with conversion efficiency over 60%.

Others [1,10] reported research in non-catalytic filtrational combustion for the conversion to syngas of wet ethanol, jet-fuel (Jet-A) and butanol. The experimental and numerical results with wet ethanol (ethanol that has only been partially distilled and dehydrated) over a range of equivalence ratios, inlet velocities, and water fractions, indicated that wet ethanol can be effectively converted to syngas in a non-catalytic filtration reactor, thus negating the necessity of complete dehydration and distillation to dry ethanol, demonstrating that this fuel is a promising biological source for hydrogen. The results also showed that the conversion of ethanol to syngas by filtrational combustion is similar to the conversion of n-heptane and methane, in terms of the behaviour of the combustion as a function of the equivalence ratio and the inlet velocity. In the case of experimental research with Jet-A and butanol, the results showed that approximately 42% of the hydrogen of the Jet-A was converted to H_2 and that 56% of the carbon was converted to CO. The H_2 yield continued to increase with φ in the experiments with Jet-A, whereas with butanol the yields of H_2 and CO both reached a maximum within the operating range studied. The peak CO yield with butanol was 72% and for H_2 it was 43%. The main products were H_2 and CO, however, CH_4, C_2H_2 and C_2H_4 were also observed in considerable quantities for both fuels, especially in experiments with butanol at φ greater than 3.0.

Decalin is a two-fused ring cycloparaffin, which is found in liquid fuels (jet fuels, diesel). It is a model compound for bicyclic naphthenes found in jet fuels and coal-, oil-shale-, tar-sand derived fuels, and it is also a potential endothermic fuel for hypersonic flight [11]. The importance of decalin in this study lies in the fact that has structural proximity to the average chemical species that can be found in a heavy fuel oil [12] and because it has been found that in mixture (methylnaphthalene/decalin/cyclohexane/*n*-hexadecane) is a promising surrogate of this fuel in combustion process [13]. Moreover, the development of semi-detailed chemical kinetic reaction mechanisms, based on lumped reactions and species for simplified description of the formation of decomposition products, which includes both low- and high-temperature chemistry, allow to study the oxidation and pyrolysis of decalin on a wide range of conditions of pressure, equivalence ratio and temperatures [14].

The main objective of this work is to present a phenomenological model for rich combustion of heavy fuel oil No. 6 in a packed-bed reactor using decalin as a model compound, and to compare the results with some experimental values. We considered a simple kinetic global scheme for the partial oxidation reforming (POR), and perform a validation with experimental data of temperatures and concentrations of gaseous products for a reactor containing IPM. Equilibrium calculations were made using the lumped reaction mechanism developed for Dagaut et al. [14]. In the following, we first describe the experimental arrangement, then the mathematical model, and then some results and discussion.

Experimental equipment and procedure

Experiments were performed using heavy fuel oil No. 6 in a packed-bed reactor. Fig. 1 shows a diagram of the

experimental reactor used. The reactor housing consisted of a 15.41 cm ID and 16.83 cm OD carbon steel pipe (0.71 cm wall thickness), which was insulated both internally and externally. The internal and external insulation thicknesses were 0.6 cm and 1.2 cm respectively, which a final internal reactor diameter of 14.21 cm, as shown in Fig. 1. At the system inlet there was a 25 cm long mixing zone prior to the 35 cm long packed bed. The packed bed consisted of 6.0 mm solid alumina spheres and had a porosity of about 40%. Liquid fuel oil No. 6 (FO 6) was injected at the top of the mixing chamber. Air was injected through a lateral side port, to allow for mixing of the fluids prior to entering the porous zone. The air was heated before entry with an electrical resistance heater. Prior to injection of FO 6, the bed was heated by combustion of LPG, as explained shortly. The average reactor pressure was 2 bar.

The temperature and pressure of the injected air were 81.7 °C and 2 bar, with a flow rate of 70 L/min (referenced at 1 bar and 20 °C). The FO 6 was injected as a constant liquid jet with a flow rate of 0.008 L/min, with injection temperature and pressure of 130 °C and 4 bar. The elemental composition of the FO 6 in mass fraction of each element was as follows: C = 0.866, H = 0.106, S = 0.020 and O = 0.004. This composition corresponds to an equivalence ratio φ of 1.3. The effluent was sampled at a distance of 4 cm from the outlet, below thermocouple T1.

In general, the temperature measurements [15] correspond to values between gas temperature (T_g) and solid temperature (T_s). In this experiments five type S thermocouples were used to measure the temperature (T1 to T5), with separations as shown in Fig. 1. Table 1 shows values of boiling temperature (T_b) and autoignition temperature (T_{AI}) of decalin and FO 6.

To start the reactor, a mixture of LPG and air with an equivalence ratio of 1.2 and a total flow rate of 100 L/min (referenced at 20 °C and 1 bar) was injected into the mixing chamber, and ignited at the reactor exit. The LPG was controlled by Aalborg mass flow controller (GFC 17). The air supply was controlled by a flow control valve with manual actuation and the flow rate was read by a rotameter. The total flow rate was then changed to 135 L/min with an equivalence ratio of 0.8, generating a change of slope in the thermal profile and higher temperature. After the combustion front had moved to the T4 zone, the flow of LPG was terminated, and the injection switched to hot air and FO 6. The sampling of the effluent was started when the temperature recorded by T3 became constant, approximately 960 s after the injection of FO 6. The temperatures in the reactor during a typical run are shown in Fig. 2. This thermal information along with the product concentrations was used in the validation of the model. Note that the vertical line represents the time at which the injection of FO 6 was started.

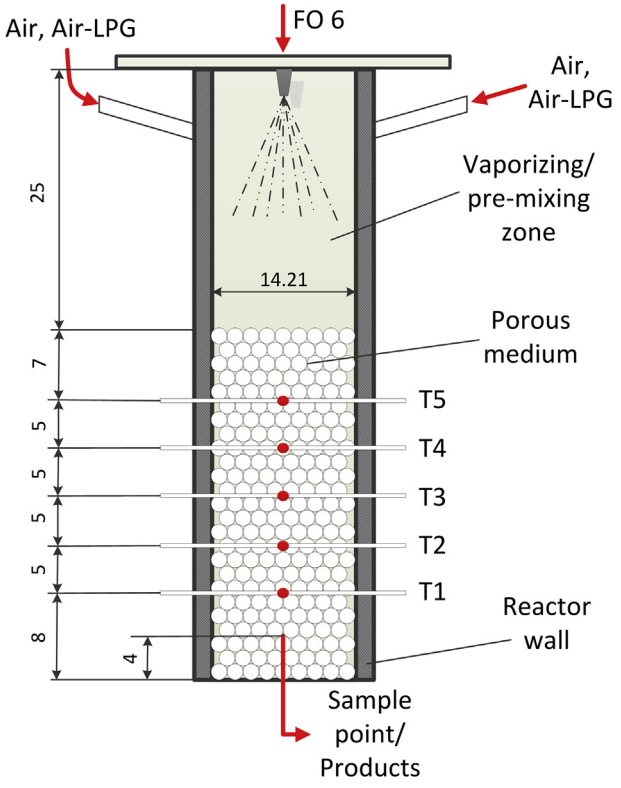

Fig. 1 – Configuration of the reactor for partial oxidation of liquid fuels. Dimensions in cm.

Mathematical model

Model overview

A detailed mathematical model was developed for the process using the conservation equations and physical property submodels equations presented by Hayes and Kolaczkowski [16]. For all of the modelling work, decalin was selected as a model compound. Using a single model compound as a first step adds simplicity to the model. The porous length was divided into two sections, called L_1 and L_2 as shown in Fig. 3. The atomized fuel and hot air are mixed in the mixing chamber, the resulting mixture enters the zone L_1. The liquid is assumed to be vaporized in this zone, and no reaction is assumed to occur. The length L_1 was established based on the boiling temperatures of the model compound and the experimental liquid fuel, assuming a total phase change. In Zone L_2 the partial oxidation of the model compound decalin in gas phase occurs. This L_2 section corresponds to the computational domain of the packed bed reactor model.

The porous medium was modelled as a continuum. The gas and solid phases are not in local thermal equilibrium, and therefore, an energy balance was written for each phase. The model was thus a heterogeneous 2D axi-symmetric transient continuum model for a packed bed reactor. We used a 2D

Table 1 – Thermal properties of decalin and FO 6.

Fuel	T_b (K)	T_{AI} (K)
$C_{10}H_{18}$	496.6[a]	523.15[b]
FO 6[c]	453.15	680.15

[a] http://webbook.nist.gov/cgi/cbook.cgi?Name=decalin&Units=SI, to 200 kPa.
[b] http://www.sigmaaldrich.com/catalog/product/sial/d251?lang=es&region=CL.
[c] http://ww2.copec.cl/combustibles/products/combustible-n5-n6.

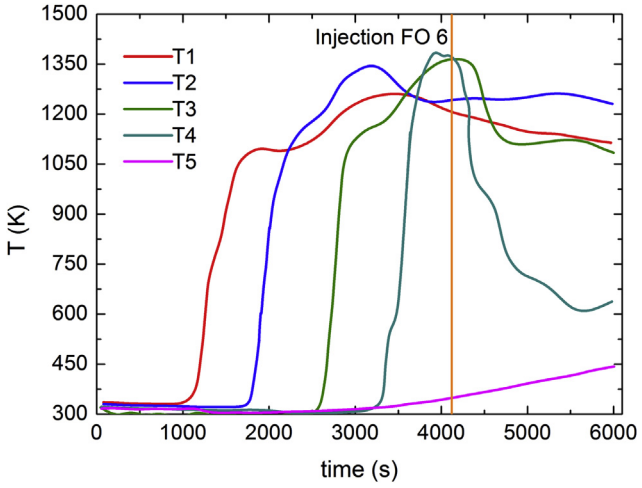

Fig. 2 – Experimental temperatures obtained during an experiment with $\varphi = 1.3$.

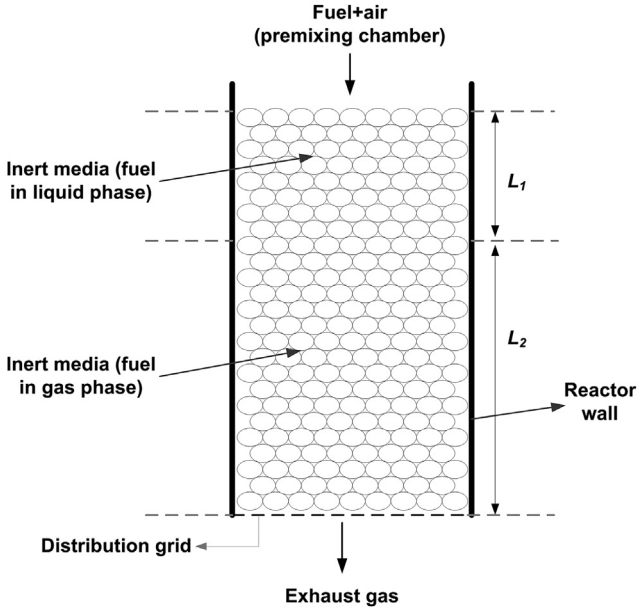

Fig. 3 – Diagram of the computational domain.

approximation because the diameter reactor is greater than 15 particle diameters [16]. The pre-heated fuel-air mixture was considered to be well mixed when it entered the porous zone. The conservation equations with corresponding boundary conditions are given in the following sections. A more detailed description of the model is available in the Supplementary information.

Momentum balance in porous medium

We used a continuum model for the packed bed. The pressure and velocity are calculated from the volume averaged Navier–Stokes (VANS) and continuity equations (momentum balance) [17]:

$$\frac{\rho_f}{\phi}\frac{\partial \mathbf{u}}{\partial t} = \nabla\cdot\left[-p\mathbf{I} + \frac{\mu}{\phi}\left(\nabla\mathbf{u} + (\nabla\mathbf{u})^T\right) - \frac{2\mu}{3\phi}(\nabla\cdot\mathbf{u})\mathbf{I}\right] - \frac{\mu}{K}\mathbf{u} \quad (1)$$

$$\frac{\partial\left(\phi\cdot\rho_f\right)}{\partial t} + \nabla\left(\rho_f\mathbf{u}\right) = 0 \quad (2)$$

Note that in keeping with typical use of the VANS in modelling flow through porous medium, the fluid phase inertial term is not retained (Brinkman style). Here $\mathbf{u}$ is the superficial velocity vector. At the inlet a normal inflow velocity was imposed, and at the outflow a constant pressure condition was set. At the wall, no-slip boundary conditions were used.

Mass balance equation for compound i in the fluid

The two dimensional axi-symmetric mass balance for component i contains terms for advection (right hand side), dispersion and source terms (both on the left hand side). It can be written as:

$$\frac{1}{r}\frac{\partial}{\partial r}\left(rD_{er}\,\rho_f\frac{\partial w_{i,f}}{\partial r}\right) + \frac{\partial}{\partial z}\left(D_{ea}\,\rho_f\frac{\partial w_{i,f}}{\partial z}\right) - (-R_i)\phi = \rho_f\left(\frac{\partial w_{i,f}}{\partial t} + u_r\frac{\partial w_{i,f}}{\partial r} + u_z\frac{\partial w_{i,f}}{\partial z}\right) \quad (3)$$

The effective dispersion coefficient in packed bed (D_e) has a radial component (D_{er}) and an axial component (D_{ea}). The initial conditions used were a specified mass fraction for the reactants and products. The boundary conditions were zero radial flux at the centreline and wall, and zero axial flux at the outlet. At the domain inlet, the Danckwerts condition was used. For both radial and axial directions, the value of the dispersion coefficient does not depend on the species [16].

Energy balance equation for the fluid

The energy balance for the fluid includes advection (right hand side) and dispersion (left hand side). It also contains source terms for reaction and heat transfer with the solid. The fluid phase energy balance is thus written:

$$\frac{1}{r}\frac{\partial}{\partial r}\left(rk_{rf}\frac{\partial T_f}{\partial r}\right) + \frac{\partial}{\partial z}\left(k_{af}\frac{\partial T_f}{\partial z}\right) - \phi\sum_{j=1}^{N_f}\Delta H_{R,j}(-R_j) - h_{fs}a_v(T_f - T_s) = \rho_f\,C_{P,f}\left(\phi\frac{\partial T_f}{\partial t} + u_r\frac{\partial T_f}{\partial r} + u_z\frac{\partial T_f}{\partial z}\right) \quad (4)$$

The fluid thermal conductivity in packed bed (k_f) has a radial component (k_{rf}) and an axial component (k_{af}). The heat transfer by radiation in the gas phase was considered negligible compared to the radiation transfer in the solid phase. The heat transfer area per unit bed volume is expressed in terms of the particle diameter and the bed porosity, that is:

$$a_v = \frac{6(1-\phi)}{D_P} \quad (5)$$

The initial fluid temperature was an approximated representation of the experimental values determined from the experiments following pre-heating by LPG combustion. The

following boundary conditions were used. At the inlet to the L_2 porous bed, the temperature was imposed as a Danckwerts condition. At the outlet, a zero axial flux condition was imposed, and a zero radial flux condition was used at the centreline. At the wall, the radial heat flux equals the heat loss to the surroundings from the fluid zone. This condition gives rise to:

$$-k_{rf}\frac{\partial T_f}{\partial r} = U_f(T_f - T_\infty) \quad \text{at} \quad r = R \tag{6}$$

Energy balance equation for the solid

The solid phase energy balance includes the effects of axial and radial conduction, as well as transfer to the fluid. The conservation equation is:

$$\frac{1}{r}\frac{\partial}{\partial r}\left(rk'_{rs}\frac{\partial T_s}{\partial r}\right) + \frac{\partial}{\partial z}\left(k'_{as}\frac{\partial T_s}{\partial z}\right) + h_{fs}a_v(T_f - T_s) = (1-\phi)\rho_s C_{P,s}\frac{\partial T_s}{\partial t} \tag{7}$$

Heat transfer by radiation in the solid phase is incorporated into the effective thermal conductivities. The modified solid thermal conductivity (k'_s) has a radial component (k'_{rs}) and an axial component (k'_{as}). The initial temperature profile is approximated according to the experimental profile that was achieved from the pre-heating with LPG combustion. The boundary conditions were zero axial flux at the inlet and outlet planes, and zero radial flux at the centreline. At the wall, the radial heat flux equals the heat loss to the surroundings from the solid zone. This condition gives rise to:

$$-k'_{rs}\frac{\partial T_s}{\partial r} = U_s(T_s - T_\infty) \quad \text{at} \quad r = R \tag{8}$$

Constitutive equations

The conservation equations contain many physical parameters which require sub-models to describe them. Appropriate definitions were used for the calculation of the overall heat transfer coefficients, fluid/solid heat transfer coefficient [18], dispersion coefficients [16,19], thermal conductivities [20,21], bed to wall heat transfer coefficients [16,22,21] and permeability of the porous media [23–25]. All gas phase species were modelled as ideal gases. The equations used in the sub-models are given in the Supplementary information.

Homogeneous reactions

We used an inlet molar ratio for decalin:oxygen = 1:6.5 based on a global balance from the semi-detailed kinetic modelling of decalin oxidation and pyrolysis described by Dagaut et al. [14]. Additional formation of hydrogen in conversion of liquid hydrocarbon fuels to syngas through filtration combustion would result from the consumption of water, produced after the initial partial oxidation reactions, through the steam reforming process occurring downstream of the main reaction zone [6]. Based on this, the proposed homogeneous reactions occurring in the packed bed reactor are:

$$C_{10}H_{18} + 6.5\ O_2 \xrightarrow{k_1} 10\ CO + 3\ H_2O + 6\ H_2 \tag{9}$$

$$2CO + O_2 \underset{k_{-2}}{\overset{k_2}{\rightleftharpoons}} 2CO_2 \tag{10}$$

$$C_{10}H_{18} + 10\ H_2O \underset{k_{-3}}{\overset{k_3}{\rightleftharpoons}} 10CO + 19\ H_2 \tag{11}$$

$$CO + H_2O \underset{k_{-4}}{\overset{k_4}{\rightleftharpoons}} CO_2 + H_2 \tag{12}$$

The kinetic expressions for Eqs. (9)–(11) that describe the transformation of the kth component due to jth reaction were derived following the methodology of Dobrego, who studied partial oxidation of methane in an inert porous media [26]. For Eq. (12) the kinetics expressions follow the development of Graven and Long [27].

There is no published information about a global chemical kinetics model for the partial oxidation and steam reforming of decalin in inert porous media. For this reason, the model was based on the available kinetic information for methane along with the one of water gas shift reaction kinetics under non-catalytic conditions, as given in Table 3 [28,26,29,27].

The kinetic constants fir the reverse reactions, k_{-2} and k_{-3}, were obtained considering chemical equilibrium [26] and followed the methodology of Hayes and Kolaczkowski [16]. The heats of reaction of Eqs. (9)–(12) were calculated from data in Hayes and Kolaczkowski [16]. The complete details about the kinetic model are given in the Supplementary information.

Computer simulation

Model solution and physical parameters

The mathematical model described in the previous section was implemented in a commercial software tool, COMSOL Multiphysics version 5.0. The simulation was performed in the domain where the species would be in gas phase. Grid refinement studies were performed to verify a mesh independent solution. The final mesh used 3271 elements. The simulated and experimental results were compared, using combustion temperature at thermocouple positions along the domain and chromatographic results of the species present at the sample point.

Mesh independence was tested by analysing the effect of the number of finite elements (element size) in the calculation domain on the mass fraction of H_2 (wet basis) at the sample point and the axial profile of this mass fraction. With an element size corresponding to 3271 elements, consistent results were obtained in terms of accuracy. Simulation data were extracted along the axis and along the radius at a position corresponding the sampling location. In addition, equilibrium results for an adiabatic process at constant pressure were calculated using CANTERA [30].

It is known that the influence of Eq. (10), oxidation of CO to CO_2, is limited in rich combustion [26], although the reaction is important. In this work, we modified the value of the

activation energy for the CO oxidation reaction by increasing the activation energy shown in Table 3 by a factor of three (to 15,000 K). A good behaviour of the thermal profile in both phases, showing an ignition zone and a moving combustion front was obtained with this value.

Fig. 2 shows the experimental temperatures before and after the injection of FO 6. The different behaviour after injection of FO 6 is noted. For example, T4, generally decreases during the process, always keeping a value below the temperature observed at the moment of injection (initial condition). For T2, the temperature evolves with a slight positive slope with respect to the temperature at moment of injection. To model the reactor behaviour in COMSOL, the initial temperature of the solid was set equal to the measured temperature profile obtained prior to the injection of FO 6, whilst the fluid temperatures were to a value that was 5% lower. This is justified because the experimental measurements of both temperatures indicate that immediately prior to the reaction zone, both phases do not have the same temperature [15], and in particular, in the results for the case of rich combustion of liquid fuel (heptane) it is observed that the gas temperature is lower than the solid temperature prior to the reaction zone [6].

The physical and homogeneous reactions parameters used in the model are given in Tables 2 and 3. The NIST database [34] is an important source of thermophysical parameters and variables utilized in the simulation. The thermal properties of the solid phase, e.g. thermal conductivity and heat capacity, were obtained from Bubnovich and Toledo [31].

Table 2 – Physical parameters.

Parameter	Source	Unit	Value
p_{out}	Experimental	bar	2
$T_{f,in}$	Experimental	K	500.15
T_∞	Experimental	K	298.15
ϕ	[31]	–	0.4
ρ_s	[31]	kg/m^3	3987
D_p	Experimental	m	6×10^{-3}
L_2	Experimental	m	0.275
v_s	Experimental	m/s	0.077
σ	[32]	W/(m^2 K^4)	5.6705×10^{-8}
R_g	[32]	J/(mol K)	8.314
$w_{C_{10}H_{18},in}$	Experimental	–	0.095
$w_{O_2,out}$	Experimental	–	0.211
D_{Ti}	Experimental	m	0.142
D_T	Experimental	m	0.154
D_o	Experimental	m	0.168
D_{oi}	Experimental	m	0.192
ε	[31]	–	0.45
ε'	[a]	–	0.7
T_o	Experimental	K	420.15
h'_o	[b]	W/(m^2 K)	4.86
k_W	[c]	W/(m K)	55
k_{i1}	[d]	W/(m K)	0.18
k_{i2}	[d]	W/(m K)	0.18

[a] http://www.rsifibre.com/pdfs/Ceramic_Fiber_Technical_Bulletin.pdf.
[b] Calculated as [32], p. 445.
[c] Carbon steel [33], p. 510.
[d] http://www.ceramaterials.com/ceramicfiberpaper.html 1,2: ceramic fiber.

Table 3 – Homogeneous reaction parameters.

Parameter	Source	Unit	Value
A'_1	[26]	m^3/(mol s)	16×10^{18}
E'_1/R_g	[26]	K	59,000
A'_2	[26]	(1/s) (m^3/mol)^2	5×10^4
E'_2/R_g	[26],[a]	K	15,000
A'_3	[26]	m^3/(mol s)	2.5×10^{20}
E'_3/R_g	[26]	K	59,000
A'	[27]	m^3/mol	3.6
B'	[27]	m^3/mol	12
k'_4	[27]	(1/s) (m^3/mol)$^{1/2}$	1.5811×10^{11}
E_4/R_g	[27]	J/mol	281,580
A'_{-4}	[27]	(1/s) (m^3/mol)$^{1/2}$	3.0042×10^9
E_{-4}	[27]	J/mol	238,488

[a] Adjusted from the value quoted in the reference.

Results and discussion

Using the discrete information for the temperature profile at moment of the injection of FO 6 shown in Fig. 2, it is possible to generate a complete initial thermal profile by piecewise cubic interpolation and constant extrapolation. The continuous result obtained is shown in Fig. 4.

The result in Fig. 4 was used to define the domain of calculation. The procedure consists in comparing the boiling temperatures between simulated and experimental fuels. The boiling temperature of decalin is greater than that of FO 6, therefore, this value for decalin is used as a criterion to define the length that ensures the total evaporation of the fuel. The location of this point in Fig. 4 establishes the length of the computational domain of calculation. For the simulated experiment, the length to ensure evaporation, according to the initial profile obtained with LPG, extends for 7.5 cm, and therefore the calculation domain (L_2) is reduced to 27.5 cm. After injection of FO 6, thermocouples that are in the domain of computation correspond to T1 and T4, therefore these

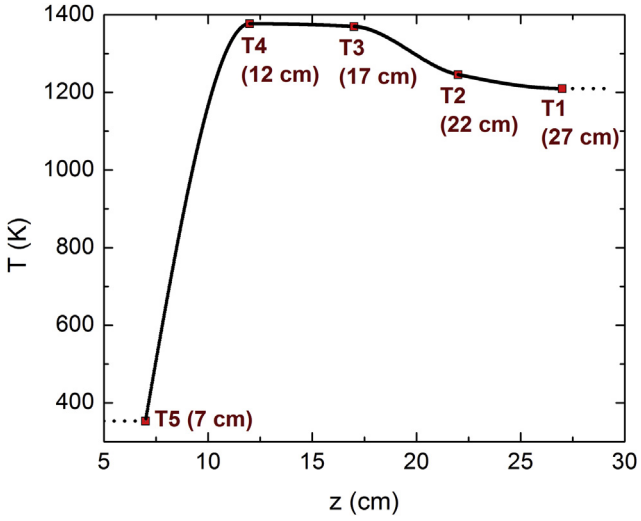

Fig. 4 – Initial thermal profile at injection FO 6 (t = 4120 s; temperatures: T1 = 1210 K, T2 = 1246 K, T3 = 1370 K, T4 = 1377 K, T5 = 353 K).

temperature data were used for comparison with the results of the simulation.

An equivalence ratio of 1.3 corresponds to inlet mass fractions of $w_{C_{10}H_{18}} = 0.095$, $w_{O_2} = 0.211$ and $w_{N_2} = 0.694$. The experimentally measured concentrations of the species in the exhaust gases are shown in Table 4. The chromatographic analysis only detects CH_4, CO_2, CO, H_2 and N_2. The results are reported on a dry basis. The percentage of N_2 is obtained from the total mass balance, to complete the information about molar fractions of the species (dry basis). The mass fractions (wet basis) obtained by simulation were converted to a dry basis. The experimental and simulation results for φ of 1.3 are shown in Table 5.

Table 5 shows the presence of H_2, CO and CO_2 in both the experiments and in the simulation. The simulation results indicate that decalin and oxygen were converted in 93.9% and 100% at the sample point, respectively.

Comparing the second and fourth columns in Table 5, we note that the simulation predicts exactly the H_2 mass fraction but the CO concentration is less well predicted. This last result could indicate that the rich filtration combustion of FO 6 might generate hydrocarbon species with molecular weights higher than those that could be detected by the present instrumental analyses. If the assumption is correct, the CO experimental concentration would decrease and give better approximation to the simulated value. The detection of different hydrocarbons in exhaust gases is typical from filtration combustion of liquid fuel in rich conditions [6,10]. The equilibrium composition of the exhausted gases is represented almost entirely for the species in fifth column in Table 5. The equilibrium calculation predicts that CH_4 is not present in the products like in experimental results. Furthermore, in this simulation decalin has predicted only some of the combustion products obtained in partial oxidation of the heavy fuel oil No. 6, because this model compound does not represent all of the initial complex chemistry of the fuel [12].

Table 4 – Chromatographic results of FO 6.

Gas	% (v/v)	Molar fraction (dry basis)
H_2	9.98	0.0998
CO	15.85	0.1585
CH_4	0.00	0.0000
CO_2	4.47	0.0447

Fig. 5 shows the axial variations of the temperatures in both phases and the concentrations (dry basis) of reactants and products (H_2 and CO). Fig. 5A and B corresponds to a time near to the FO 6 injection time (4380 s). At this time the maximum measured temperature was 1341 K at 17 cm from the inlet of the packed bed. This time was selected to observe the predictive capacity of the model with respect to the higher temperatures measured during filtration combustion of FO 6. The model predicted $T_f = 1250$ K in this location at this time.

Fig. 5C and D corresponds to the same above information occurring at the instant of gas sampling (5080 s). It is observed that the thermal profiles in both phases are coincident, indicating an efficient energy exchange between the phases. The constant behaviour of T2 as predicted by the model and the simulation is near to T1 in Fig. 5A. Furthermore, the simulation results seen when comparing Fig. 5A and C indicates that the overall heat profile has a movement upstream, observed by the beginning of the change of curvature of the right branch in the time interval considered. Also, the experimental temperatures observed in Fig. 2 show that the net heat flux points in the upstream direction. This indicates that the front it is moving into a relatively cool solid, with maximum temperature in the wave less than the adiabatic temperature [10,35], whose value to decalin is 2292 K, calculated by CANTERA and using the semi-detailed kinetic reaction mechanism for decalin oxidation and pyrolysis developed for Dagaut et al. [14]. It is observed in Fig. 5A and C that the autoignition of decalin occurs upstream of T2 with an abrupt decrease in the decalin and oxygen concentrations.

Peak temperatures approximately coincide with peaks in H_2 production along the packed bed as can b seen in Fig. 5B and D. For example, in Fig. 5D the maximum mass fraction of H_2 is 0.011 at z = 14.6 cm and the peaks of gas and solid temperatures are 1294.5 K (z = 15.07 cm) and 1293.1 K (z = 15.09 cm), respectively. This zone with a H_2 peak could be explained considering two effects observed by simulation. In the middle of this source zone the overall reaction rate of hydrogen is maximum at 0.003 kg/($m^3 \times s$) and the zone has an endothermic behaviour as shown the overall reaction heat in Fig. 5C, promoting the steam reforming from decalin and its conversion to hydrogen ($k_3 \gg k_{-3}$).

The marked decreases in temperatures T3 and T4, seen when comparing Fig. 5A and C, are note well predicted by the model. These abrupt decreases could indicate the possible

Table 5 – Experimental and simulated mass fractions of gas phase species.

Gas	Experimental mass fraction (dry basis)	Simulation mass fraction (wet basis)	Simulation mass fraction (dry basis)	Equilibrium mass fraction (dry basis)[a]
$C_{10}H_{18}$	–	0.0058	0.0062	4.7182×10^{-116}
O_2	–	2.3442×10^{-9}	2.4941×10^{-9}	6.3948×10^{-5}
H_2	0.0076	0.0071	0.0076	0.0020
N_2	0.7472	0.6433	0.6844	0.7651
CO	0.1699	0.0873	0.0929	0.0952
CH_4	0.0000	–	–	2.0316×10^{-13}
CO_2	0.0753	0.1964	0.2090	0.1370
H_2O	–	0.0601	–	–
∑	1	1	1	0.9994

[a] Calculated by CANTERA [30] with kinetic reaction mechanism for decalin oxidation and pyrolysis [14] at 500.15 K, 2 bar and φ = 1.3.

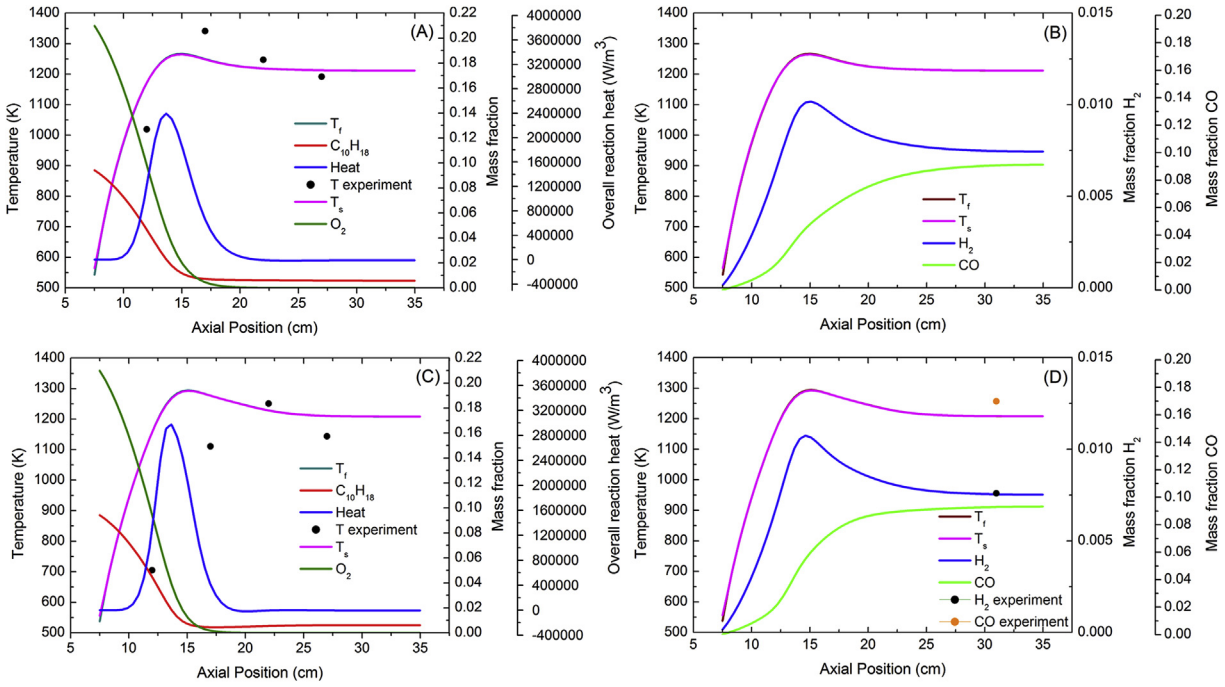

Fig. 5 – Simulations and experimental axial variations at two instants after FO 6 injection: near to injection, t = 4380 s (A and B); and at sampling of exhaust gases, t = 5080 s (C and D).

presence of liquid fuel boiling at this location near the reactor inlet, considering that the fuel was injected as a constant liquid jet. This situation would explain the deviation in the temperature profiles from simulation results which are based only on continuous modelling in the phase gas. Experimentally we observed the presence of an agglomerated carbonaceous residue in the porous medium possibly formed by generation of soot, coke and presence of liquid fuel. Formation of soot has been observed in conversion of jet fuel and butanol to syngas by filtration combustion [10]. The formation of coke through heat cracking and subsequent evaporation of the lighter components, and the formation of soot particles as the result of gas phase chemical reactions could reduce or cancel the packed bed porosity in some regions, as well as create an additional heat transfer resistance on the alumina beads forming the porous media, resulting in inefficiency of the process of recirculation of heat that allows the solid phase, affecting the stability of the flame front, and the production of syngas. In large scale applications of rich filtration combustion would be necessary to consider both the burned with a lean mixture which propagates downstream through the reactor and would be required in addition to a cleaning procedure [10].

Fig. 6 shows the radial variation of temperatures in both phases and the radial profile of H_2 concentration in dry basis, for the time and location of the gas sampling (z = 31 cm). It is observed that the radial variations for the temperatures are $\Delta T_f = -1.94$ K and $\Delta T_s = -3.01$ K between centre and radius of the packed bed, and the variation of H_2 mass fraction is negligible. The different variation between gas and solid thermal profile near the inner wall can be explained by the magnitude of the overall heat transfer coefficient at this location ($U_s > U_f$).

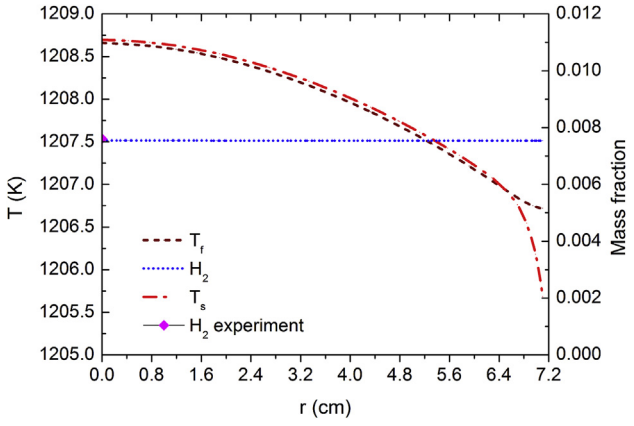

Fig. 6 – Radial variation of gas and solid temperatures and H_2 mass fraction at sampling point.

Figs. 7–9 show by simulation the impact of the equivalence ratio, filtration velocity and heat loss on H_2 production at the sampling point. These graphs also include the maximum axial temperature predicted at sampling point. The simulation shown in Fig. 7 was performed using the physical parameters given in Table 2. The effect of varying the equivalence ratio in the interval 1 to 4 was studied. It was observed that the mass fraction of hydrogen in the products increase with equivalence ratio and this can be attributed to the increase of fuel inlet concentration because the combustion temperature stays constant at the equivalence ratio range.

Fig. 8 shows the effect of the filtration velocity on the H_2 production at the sampling point and the axial maximum temperature for $\varphi = 2.2$. Fig. 8 shows an increasing trend in

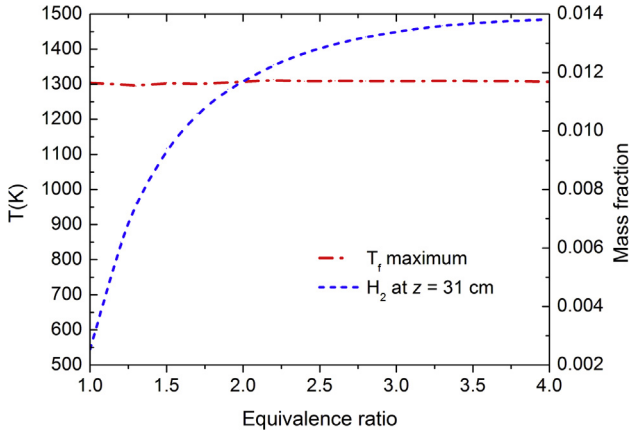

Fig. 7 – H_2 concentration in dry basis and axial maximum T_f on equivalence ratio.

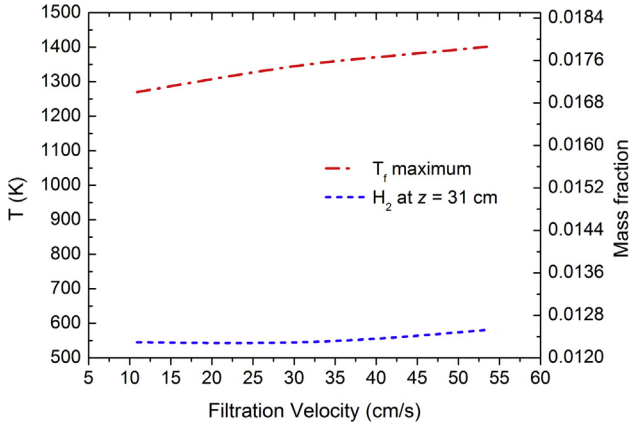

Fig. 8 – Peak temperatures and H_2 concentration as a function of filtration velocity at $\varphi = 2.2$.

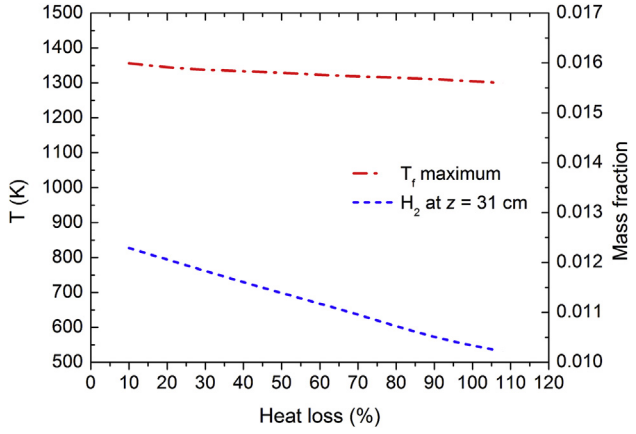

Fig. 9 – Effect of heat loss on the combustion temperature and H_2 production.

combustion temperature with an increase in the filtration velocity. Experimental and simulation results to for liquid heptane show a similar behaviour [6]. This trend is explained through simulation by the increase in the thermal conductivities of both phases and interfacial heat transfer. Also, it is observed that the H_2 concentration at the sampling point does not change significantly over the filtration velocity range of 10–55 cm/s.

Fig. 9 shows the effect of the heat loss on the maximum axial temperature and the H_2 concentration at the sampling point. For this analysis $\varphi = 2.2$ and $v_{filt} = 32.7$ cm/s was selected. It is observed that the increase in heat loss generates a decrease of the combustion temperature with the consequent decrease in the production of H_2.

In general, the implications and applications of the results point to the use of pure model compounds and mixtures of these, as surrogate fuels, allowing the prediction of the combustion behaviour of more complex liquid fuels, in addition to providing standardized fuels that do not change over time, and which serve as a pattern of these fuels [36]. In particular, it is interesting to propose the use of decalin in mixtures of surrogate fuels, and allowing the mathematical simulation of the kinetic behaviour during rich filtrational combustion of liquid fuels complex as heavy fuel oil, diesel, jet fuel, among others, in their application for the production of H_2/syngas.

Conclusions

In this paper we have described a methodology and validation for a model for the production of syngas from heavy fuel oil. The approach of 2D bed packed modelling proposed in this work, using decalin as a model compound, allows a reasonable representation of the key characteristics and trends observed in rich filtration combustion of heavy fuel oil. The proposed kinetic global model for the homogeneous gas phase POR of decalin gave a close prediction of the experimental H_2 production for specific operating conditions at equivalence ratio $\varphi = 1.3$. The radial variations of this concentration were not observed to be significant at the sampling point.

The simulation results show notable characteristics of the process, such as the presence of an axial maximum in the production of H_2, and the positive effects of the increase of the equivalence ratio and filtration velocity on concentration of this combustion product. Finally, a reduction in heat losses would allow higher combustion temperatures which would achieve greater fuel conversions to H_2.

The kinetic global model for partial oxidation reforming of decalin proposed in this work and used in simulations of filtration combustion of a heavy fuel oil in rich conditions gives similar results to the experimental production of H_2. This evidence suggests that the use of decalin as model compound subject to the set of homogeneous reactions described is suitable for future studies with surrogate mixtures that include this chemical component to describe rich filtration combustion of heavy fuel oils. The proposed POR model can be used to suggest new ways of controlling and optimizating of the H_2 production, and technologically in the design and scale-up of these packed bed reactors.

Acknowledgements

The authors are grateful for financial support from CONICYT-Chile (FONDECYT 1121188, PCHA/Doctorado Nacional/2013-

21130165) and research award ELAP-CBIE (2015) from the Government of Canada.

Nomenclature

A'	Constant in water gas shift reaction, m^3/mol
a_v	Heat transfer area per unit volume of reactor, m^{-1}
B'	Constant in water gas shift reaction, m^3/mol
C_P	Constant pressure heat capacity, J/(kg K)
D_{oi}	Reactor diameter at contact with surrounding, m
D_T	Internal diameter of the metallic tube, m
D_{Ti}	Internal diameter of the reactor defined at interface bed packed-insulation, m
D_o	External diameter of the metallic tube, m
D_p	Equivalent particle diameter, m
D_{er}	Effective radial dispersion coefficient in a packed bed, m^2/s
D_{ea}	Effective axial dispersion coefficient in a packed bed, m^2/s
E'_j	Activation energy divided by R_g in forward rate constant of jth reaction, K
E_j	Activation energy in forward rate constant of jth reaction, J/mol
E_{-j}	Activation energy in reverse rate constant of jth reaction, J/mol
ΔH_R	Heat of reaction, J/mol
h'_o	Heat transfer coefficient due to loss by free convection, W/(m^2 K)
h_{fs}	Heat transfer coefficient between fluid and solid surface, W/(m^2 K)
$\mathbf{I}$	Unit tensor, dimensionless
K	Permeability, m^2
k	Thermal conductivity, W/(m K)
k_j	Forward rate constant of jth reaction, various units
k_{-j}	Reverse rate constant of jth reaction, various units
k'_j	Pre-exponent factor in forward rate constant of jth reaction, various units
k'_{-j}	Pre-exponent factor in reverse rate constant of jth reaction, various units
k_{af}	Axial fluid thermal conductivity in a packed bed, W/(m K)
k_{rf}	Radial fluid thermal conductivity in a packed bed, W/(m K)
k'_{rs}	Modified radial solid thermal conductivity, W/(m K)
k'_{as}	Modified axial solid thermal conductivity, W/(m K)
L	Porous length, m
N_f	Number of species in fluid phase
p	Pressure, Pa
R_i	Rate of reaction of species i by overall chemical kinetics model, kg/(m^3 s)
r	Radial coordinate in cylindrical coordinate system, m
R_g	Universal gas constant, 8.314 J/(mol K)
R	Radius of packed bed, m
t	Time, s
T_o	Temperature at interface insulation-surroundings, K
T	Temperature, K
T	Experimental temperature, K
$\mathbf{u}$	Velocity field, m/s
U_f	Overall heat transfer coefficient for fluid based on the inside area of the reactor, W/(m^2 K)
U_s	Overall heat transfer coefficient for solid based on the inside area of the reactor, W/(m^2 K)
v_s	Mass average superficial fluid velocity, m/s
v_{filt}	Filtration velocity, m/s
w	Mass fraction of species i, dimensionless
z	Axial coordinate in cylindrical coordinate system, m

Greek symbols

ε	Particle emissivity, dimensionless
ε'	Insulation emissivity, dimensionless
μ	Viscosity, Pa s
ρ	Fluid density, kg/m^3
σ	Stephan–Boltzmann constant, 5.67×10^{-8} W/(m^2 K^4)
ϕ	Porosity of porous medium, dimensionless
φ	Equivalence ratio

Subscripts

AI	Autoignition
f	Fluid
g	gas
i	Species, insulation
j	jth reaction
in	Inlet
out	Outlet
s	Solid
W	Reactor wall
∞	Surrounding

Appendix A. Supplementary data

Supplementary data related to this article can be found at http://dx.doi.org/10.1016/j.ijhydene.2016.08.111.

REFERENCES

[1] Smith CH, Leahey DM, Miller LE, Ellzey JL. Conversion of wet ethanol to syngas via filtration combustion: an experimental and computational investigation. Proc Combust Inst 2011;33:3317–24.
[2] Al-Hamamre Z, Deizinger S, Mach A, von Issendorff F, Trimis D. Thermal partial oxidation of diesel in porous reactors for synthesis gas production. Clean Air 2006;7:391–407.
[3] Babkin VS. Filtration combustion of gases, present state of affairs and prospects. Pure Appl Chem 1993;65(2):335–44.
[4] Fay M, Dhamrat R, Ellzey JL. Effect of porous reactor design on conversion of methane to hydrogen. Combust Sci Tech 2005;177:2171–89.
[5] Toledo M, Bubnovich V, Saveliev AV, Kennedy L. Hydrogen production in ultrarich combustion of hydrocarbon fuels in porous media. Int J Hydrogen Energy 2009;34:1818–27.
[6] Dixon MJ, Schoegl I, Hull CB, Ellzey JL. Experimental and numerical conversion of liquid heptane to syngas through combustion in porous media. Combust Flame 2008;154:217–31.
[7] Pedersen-Mjaanes H, Chan L, Mastorakos E. Hydrogen production from rich combustion in porous media. Int J Hydrogen Energy 2005;30:579–92.

[8] Pastore A, Mastorakos E. Rich n-heptane and diesel combustion in porous media. Exp Therm Fluid Sci 2010;34:359–65.
[9] Pastore A, Mastorakos E. Syngas production from liquid fuels in a non-catalytic porous burner. Fuel 2011;90:64–76.
[10] Smith CH, Pineda DI, Zak CD, Ellzey JL. Conversion of jet fuel and butanol to syngas by filtration combustion. Int J Hydrogen Energy 2013;38:879–89.
[11] Oehlschlaeger MA, Shen H-PS, Frassoldati A, Pierucci S, Ranzi E. Experimental and kinetic modeling study of the pyrolysis and oxidation of decalin. Energy & Fuels 2009;23:1464–72.
[12] Baert RSG. A mathematical model for heavy fuel droplet vaporization and pyrolysis in a heavy temperature inert gas. Combust Sci Technol 1993;90(1–4):125–47.
[13] Gudiyella S, Raman A, Perez P. Combustion of heavy fuel oil. In: 10th International symposium on heavy oil upgrading, production and characterization; 2013.
[14] Dagaut P, Ristori A, Frassoldati A, Faravelli T, Dayma G, Ranzi E. Experimental and semi-detailed kinetic modeling study of decalin oxidation and pyrolysis over a wide range of conditions. Proc Combust Inst 2013;34:289–96.
[15] Zheng Ch, Cheng L, Saveliev A, Luo Z, Cen K. Gas and solid phase temperature measurements of porous media combustion. Proc Combust Inst 2011;33:3301–8.
[16] Hayes RE, Kolaczkowski ST. Introduction to catalytic combustion. 1st ed. Reading: Gordon and Breach Science Publishers; 1997.
[17] Jodeiri N, Mmbaga JP, Wu L, Wanke SE, Hayes RE. Modelling a counter-diffusive reactor for methane combustion. Comput Chem Eng 2012;39:47–56.
[18] Wakao N, Kaguei S. Heat and mass transfer in packed beds. 1st ed. London: Gordon and Breach; 1982.
[19] Carberry JJ. Chemical and catalytic reaction engineering. 1st ed. Toronto: McGraw-Hill; 1976.
[20] Feyo de Azevedo S, Romero-Ogawa MA, Wardle AP. Modelling of tubular fixed-bed catalytic reactors: a brief review. Trans I Chem E Part A 1990;68:483–502.
[21] Dixon AG, Cresswell DL. Theoretical prediction of effective heat transfer parameters in packed beds. AIChE J 1979;25:663–76.
[22] Yagi S, Wakao N. Heat and mass transfer from wall to fluid in packed beds. AIChE J 1959;5(1):79–85.
[23] Fand RM, Kim BYK, Lam ACC, Phan RT. Resistance to the flow of fluids through simple and complex porous media whose matrices are composed of randomly packed spheres. J Fluids Eng 1987;109:268–73.
[24] Kececioglu I, Jiang Y. Flow through porous media of packed spheres saturated with water. J Fluids Eng 1994;116:164–70.
[25] Jafari A, Zamankhan P, Mousavi SM, Pietarinen K. Modeling and CFD simulation of flow behavior and dispersivity through randomly packed bed reactors. Chem Eng J 2008;144:476–82.
[26] Dobrego KV, Gnezdilov NN, Lee SH, Choi HK. Overall chemical kinetics model for partial oxidation of methane in inert porous media. Chem Eng J 2008;44:79–87.
[27] Graven WM, Long FJ. Kinetics and mechanisms of the two opposing reactions of the equilibrium $CO + H_2O = CO_2 + H_2$. J Am Chem Soc 1954;76:2602–7.
[28] Dobrego KV, Gnezdilov NN, Lee SH, Choi HK. Partial oxidation of methane in a reverse flow porous media reactor. Water admixing optimization. Int J Hydrogen Energy 2008;33:5535–44.
[29] Sato T, Kurosawa Sh, Smith Jr RL, Adschiri T, Arai K. Water gas shift reaction kinetics under noncatalitic conditions in supercritical water. J Supercrit Fluids 2004;29:113–9.
[30] Goodwin DG. An open-source, extensible software suite for CVD process simulation. In: Chemical vapor deposition XVI and EUROCVD, vol. 18; 2003. p. 155–62.
[31] Bubnovich V, Toledo M. Analytical modelling of filtration combustion in inert porous media. Appl Therm Eng 2007;27:1144–9.
[32] Bird RB, Stewart WE, Lightfoot EN. Transport phenomena. 2nd ed. New York: John Wiley & Sons, Inc; 2002.
[33] Ashby MF. Materials selection in mechanical design. 4th ed. Burlington: Elsevier Ltd; 2011.
[34] NIST Chemistry webbook, NIST standard reference database number 69, Available at: http://webbook.nist.gov/chemistry/ (accessed March 2015).
[35] Zhdanok S, Kennedy LA, Koester G. Superadiabatic combustion of methane air mixtures under filtration in a packed bed. Combust Flame 1995;100:221–31.
[36] Pitz WJ, Mueller Ch J. Recent progress in the development of diesel surrogate fuels. Prog Energy Combust Sci 2011;37:330–50.